Rapid Communications

Stabilizing even-parity chiral superconductivity in Sr_2RuO_4

Han Gyeol Suh,[1] Henri Menke,[2] P. M. R. Brydon,[2] Carsten Timm,[3] Aline Ramires,[4,5,6,*] and Daniel F. Agterberg[1]

[1]*Department of Physics, University of Wisconsin, Milwaukee, Wisconsin 53201, USA*

[2]*Department of Physics and MacDiarmid Institute for Advanced Materials and Nanotechnology, University of Otago, P.O. Box 56, Dunedin 9054, New Zealand*

[3]*Institute of Theoretical Physics and Würzburg-Dresden Cluster of Excellence ct.qmat, Technische Universität Dresden, D-01062 Dresden, Germany*

[4]*Max Planck Institute for the Physics of Complex Systems, D-01187 Dresden, Germany*

[5]*ICTP-SAIFR, International Centre for Theoretical Physics, South American Institute for Fundamental Research, São Paulo, SP 01140-070, Brazil*

[6]*Instituto de Física Teórica, Universidade Estadual Paulista, São Paulo, SP 01140-070, Brazil*

(Received 7 January 2020; accepted 24 June 2020; published 21 July 2020)

Strontium ruthenate (Sr_2RuO_4) has long been thought to host a spin-triplet chiral p-wave superconducting state. However, the singletlike response observed in recent spin-susceptibility measurements casts serious doubts on this pairing state. Together with the evidence for broken time-reversal symmetry and a jump in the shear modulus c_{66} at the superconducting transition temperature, the available experiments point towards an even-parity chiral superconductor with $k_z(k_x \pm ik_y)$-like E_g symmetry, which has consistently been dismissed based on the quasi-two-dimensional electronic structure of Sr_2RuO_4. Here, we show how the orbital degree of freedom can encode the two-component nature of the E_g order parameter, allowing for a local orbital-antisymmetric spin-triplet state that can be stabilized by on-site Hund's coupling. We find that this exotic E_g state can be energetically stable once a complete, realistic three-dimensional model is considered, within which momentum-dependent spin-orbit coupling terms are key. This state naturally gives rise to Bogoliubov Fermi surfaces.

DOI: 10.1103/PhysRevResearch.2.032023

Introduction. Based on early Knight shift [1], polarized neutron scattering [2], muon-spin resonance [3], and polar Kerr measurements [4], Sr_2RuO_4 has been widely thought to support a spin-triplet chiral p-wave superconducting state with E_u symmetry [5–21]. This proposed state has had difficulty reconciling other experimental results [21], including the absence of chiral edge currents [22], thermal transport consistent with a nodal state [23–25], apparent Pauli-limiting effects for in-plane fields [26], and the failure to observe a cusplike behavior of the critical temperature under nematic strain [27,28]. Plausible explanations for each of these inconsistencies have nevertheless been presented [21,29,30]. Recently, however, the Knight shift has been revisited [31,32] and, contrary to earlier results, a relatively large reduction of the Knight shift for in-plane fields in the superconducting state has been observed. This finding cannot be reconciled with the standard spin-triplet chiral p-wave state [6].

Although it now seems unlikely that Sr_2RuO_4 is a spin-triplet chiral p-wave superconductor, the observation of broken time-reversal symmetry [3,4,33] and a jump in the shear modulus c_{66} [34,35] at the critical temperature still indicate a multicomponent order parameter [36]. The only other possible multicomponent channel within D_{4h} symmetry belongs to the E_g irreducible representation (irrep) [36]. At the Fermi surface, a chiral order parameter in this channel resembles a spin-singlet d-wave state, which has horizontal line nodes. Such a state would appear to imply that the dominant pairing instability involves electrons in different RuO_2 layers, which is difficult to understand in view of the pronounced quasi-two-dimensional nature of the normal state of Sr_2RuO_4. Indeed, no microscopic calculation for Sr_2RuO_4 has found a leading weak-coupling E_g instability [37–39].

In this Rapid Communication, we show that *local* interactions can lead to a weak-coupling instability in the E_g channel, once we consider a complete three-dimensional (3D) model for the normal state. Physically, this E_g state is a local (i.e., s-wave) orbital-antisymmetric spin-triplet (OAST) state stabilized by on-site Hund's coupling. When the renormalized low-energy Hund's coupling J becomes larger than the interorbital Hubbard interaction U', this channel develops an attractive interaction [40–45]. This pairing instability has been found in dynamical mean-field theory, which predicts it appears in the strong-coupling limit even when the unrenormalized high-energy J is less than U' [46], and also in the presence of strong charge fluctuations [47]. Pairing due to this type of interaction was considered for Sr_2RuO_4 in Ref. [40], where an A_{1g} pairing state was found to be stable. Motivated by the relevance of J for the normal state of Sr_2RuO_4 [48], we revisit the local-pairing scenario. We note that, remarkably, a similar

*Present address: Paul Scherrer Institut, CH-5232 Villigen, Switzerland.

OAST pairing state is believed to be responsible for nematic superconductivity in $Cu_xBi_2Se_3$ [49–51]. In the following, we show that an E_g state can be stabilized over the A_{1g} state of Ref. [40] by including momentum-dependent spin-orbit coupling (SOC) corresponding to interlayer spin-dependent hopping with a hopping integral on the order of 10 meV. This small value leaves the quasi-two-dimensional nature of the band structure intact. Moreover, we use the concept of superconducting fitness [52,53] to understand the importance of this term in stabilizing the E_g state. Finally, we show that this chiral multiorbital E_g state will display Bogoliubov Fermi surfaces [54,55], instead of line nodes.

Normal-state Hamiltonian. An accurate description of the normal-state Hamiltonian is crucial for understanding superconductivity in the weak-coupling limit. Our starting point is a tight-binding parametrization of the normal-state Hamiltonian that includes all terms allowed by symmetry [56]. To determine the magnitude of each term, we carry out a fit to the density-functional theory (DFT) results of Veenstra *et al.* [57]. Details on the numerical procedures are provided in the Supplemental Material (SM) [58]. However, angle-resolved photoemission spectroscopy (ARPES) measurements [48,62] suggest that some DFT parameters differ appreciably from the measured values, in particular the SOC strengths [57]. We therefore allow the SOC parameters to vary in order to understand how they affect the leading superconducting instability, under the constraint that the Fermi surfaces do not differ significantly from the DFT predictions and are hence still qualitatively in accordance with the ARPES results.

The relevant low-energy degrees of freedom (DOF) are the electrons in the t_{2g}-orbital manifold d_{yz}, d_{xz}, and d_{xy} of Ru. Using the spinor operator $\Phi_{\boldsymbol{k}}^\dagger = (c_{\boldsymbol{k},yz\uparrow}^\dagger, c_{\boldsymbol{k},yz\downarrow}^\dagger, c_{\boldsymbol{k},xz\uparrow}^\dagger, c_{\boldsymbol{k},xz\downarrow}^\dagger, c_{\boldsymbol{k},xy\uparrow}^\dagger, c_{\boldsymbol{k},xy\downarrow}^\dagger)$, where $c_{\boldsymbol{k},\gamma\sigma}^\dagger$ creates an electron with momentum $\boldsymbol{k}$ and spin σ in orbital γ, we construct the most general three-orbital single-particle Hamiltonian as $H_0 = \sum_{\boldsymbol{k}} \Phi_{\boldsymbol{k}}^\dagger \hat{H}_0(\boldsymbol{k}) \Phi_{\boldsymbol{k}}$ with

$$\hat{H}_0(\boldsymbol{k}) = \sum_{a=0}^{8} \sum_{b=0}^{3} h_{ab}(\boldsymbol{k}) \lambda_a \otimes \sigma_b, \tag{1}$$

where the λ_a are Gell-Mann matrices encoding the orbital DOF and the σ_b are Pauli matrices encoding the spin (λ_0 and σ_0 are unit matrices), and $h_{ab}(\boldsymbol{k})$ are even functions of momentum. Time-reversal and inversion symmetries allow only for 15 $h_{ab}(\boldsymbol{k})$ functions to be finite. The explicit form of the $h_{ab}(\boldsymbol{k})$ functions and the Gell-Mann matrices are given in the SM [58].

Interactions and superconductivity. We consider on-site interactions of the Hubbard-Kanamori type [63],

$$\begin{aligned} H_{\text{int}} = {} & \frac{U}{2} \sum_{i,\gamma,\sigma\neq\sigma'} n_{i\gamma\sigma} n_{i\gamma\sigma'} + \frac{U'}{2} \sum_{i,\gamma\neq\gamma',\sigma,\sigma'} n_{i\gamma\sigma} n_{i\gamma'\sigma'} \\ & + \frac{J}{2} \sum_{i,\gamma\neq\gamma',\sigma,\sigma'} c_{i\gamma\sigma}^\dagger c_{i\gamma'\sigma'}^\dagger c_{i\gamma\sigma'} c_{i\gamma'\sigma} \\ & + \frac{J'}{2} \sum_{i,\gamma\neq\gamma',\sigma\neq\sigma'} c_{i\gamma\sigma}^\dagger c_{i\gamma\sigma'}^\dagger c_{i\gamma'\sigma'} c_{i\gamma'\sigma}, \end{aligned} \tag{2}$$

TABLE I. All even-parity local gap functions classified by irreps of the point group D_{4h}. Here, $[a, b]$ corresponds to the parametrization of the gap matrix as $\lambda_a \otimes \sigma_b(i\sigma_2)$. The other columns give the orbital and spin character, as well as the interaction g for each superconducting state derived from the Hubbard-Kanamori interaction H_{int} in Eq. (2). Note that the two components of the E_g order parameters can stem from the orbital DOF, as for {[2, 0], [3, 0]} and {[6, 3], −[5, 3]}, or from the spin DOF, as for {[4, 1], [4, 2]}.

Irrep	$[a, b]$	Orbital	Spin	Interaction g
A_{1g}	[0, 0]	Symmetric	Singlet	$U + 2J$
	[8, 0]	Symmetric	Singlet	$U - J$
	[4, 3]	Antisymmetric	Triplet	$U' - J$
	[5, 2] − [6, 1]	Antisymmetric	Triplet	$U' - J$
A_{2g}	[5, 1] + [6, 2]	Antisymmetric	Triplet	$U' - J$
B_{1g}	[7, 0]	Symmetric	Singlet	$U - J$
	[5, 2] + [6, 1]	Antisymmetric	Triplet	$U' - J$
B_{2g}	[1,0]	Symmetric	Singlet	$U' + J$
	[5, 1] − [6, 2]	Antisymmetric	Triplet	$U' - J$
E_g	{[2, 0], [3, 0]}	Symmetric	Singlet	$U' + J$
	{[4, 1], [4, 2]}	Antisymmetric	Triplet	$U' - J$
	{[6, 3], −[5, 3]}	Antisymmetric	Triplet	$U' - J$

where $c_{i\gamma\sigma}^\dagger$ ($c_{i\gamma\sigma}$) creates (annihilates) an electron at site i in orbital γ with spin σ, and $n_{i\gamma\sigma} = c_{i\gamma\sigma}^\dagger c_{i\gamma\sigma}$. The first two terms describe repulsion ($U, U' > 0$) between electrons in the same and in different orbitals, respectively. The third and fourth terms represent the Hund's exchange interaction and pair-hopping interactions, respectively. We take $J = J'$ [63], where $J > 0$ is expected for Sr_2RuO_4. In the context of Sr_2RuO_4, H_{int} is usually taken as the starting point for the calculation of the spin- and charge-fluctuation propagators which enter into the effective interaction [16,19]. Here, we take a different approach [40,43] by directly decoupling the interaction in the Cooper channel, which, for $U' - J < 0$, yields an attractive interaction for on-site pairing in an OAST state. This scenario has previously been applied to a two-dimensional model of Sr_2RuO_4, predicting an OAST A_{1g} state [40]. Although a strong-coupling instability towards an OAST E_g state in the absence of SOC has been predicted in Ref. [47], the superconductivity in Sr_2RuO_4 is likely in the weak-coupling regime [21]. It is therefore important to understand if an OAST E_g state can be the leading instability in this limit.

In the spirit of Ref. [43], we treat H_{int} as a renormalized low-energy effective interaction. We tabulate the allowed local gap functions, their symmetries, and the interactions in the respective pairing channels in Table I. Here, we adopt the common assumption of on-site rotational symmetry, which stipulates $U = U' + 2J$ [63]. This choice implies that all the OAST channels have the same attractive pairing interaction, which highlights the role of the normal-state Hamiltonian in selecting the most stable state. However, since the Ru sites have D_{4h} symmetry and not the assumed full rotational symmetry, the interaction strengths for the different pairing channels are generally different. Our results should therefore be interpreted as providing a guide to which superconducting states this form of attractive interaction can give rise.

We write a free-energy expansion up to second order in the superconducting order parameter given by the gap matrices $\hat{\Delta}_i = \Delta_i \lambda_{a_i} \otimes \sigma_{b_i}(i\sigma_2)$,

$$\mathcal{F} = \frac{1}{2}\sum_i \frac{1}{g_i}\mathrm{Tr}[\hat{\Delta}_i^\dagger \hat{\Delta}_i] - \frac{k_B T}{2}\sum_{\boldsymbol{k},\omega,i,j}\mathrm{Tr}[\hat{\Delta}_i \underline{\hat{G}} \hat{\Delta}_j^\dagger \hat{G}], \quad (3)$$

where i and j sum over all channels of a chosen irrep, g_i are the corresponding interaction strengths from Table I, $\omega_m = (2m+1)\pi k_B T$ are the fermionic Matsubara frequencies, and $\hat{G} = (i\omega_m - \hat{H}_0)^{-1}$ and $\underline{\hat{G}} = (i\omega_m + \hat{H}_0^T)^{-1}$ are the normal-state Green's functions. Nontrivial solutions of the coupled linearized gap equations obtained from $\partial\mathcal{F}/\partial\Delta_i^* = 0$ give the critical temperature T_c and the linear combination of the $\hat{\Delta}_i$ corresponding to the leading instability. We include all channels in a chosen irrep, not just the attractive ones (see Table I). In evaluating the last term in Eq. (3), we keep only intraband contributions; although the inclusion of interband terms will shift T_c, this effect is negligible in the weak-coupling regime, as discussed in detail in the SM [58].

Results. Weak-coupling OAST pairing states for an attractive Hund's interaction require nonvanishing SOC [43,44,53]. As described in the SM [58], SOC appears in five terms in the Hamiltonian $\hat{H}_0(\boldsymbol{k})$ in Eq. (1), representing a large parameter space to explore. We shall focus on the effects of the following terms: the z component of the atomic SOC, $h_{43} = \eta_z$; the in-plane atomic SOC, $h_{52} - h_{61} = \eta_\perp$; and the momentum-dependent SOC associated with the interlayer hopping amplitude t_{56z}^{SOC} between the d_{xy} and the d_{xz} and d_{yz} orbitals, $\{h_{53}, h_{63}\} = 8\, t_{56z}^{\mathrm{SOC}} \sin(k_z c/2)\{\cos(k_x a/2)\sin(k_y a/2), -\sin(k_x a/2)\cos(k_y a/2)\}$. Here, we will ignore the anisotropy of the atomic SOC and set $\eta_z = \eta_\perp = \eta$. We have carried out a cursory exploration of the larger SOC parameter space and find that varying the other parameters within reasonable ranges such that the Fermi surfaces do not significantly deviate from the DFT predictions has little effect on the leading instability.

Figure 1(a) shows the phase diagram as a function of the atomic SOC η and the momentum-dependent SOC, parametrized by t_{56z}^{SOC}. We find leading instabilities in the A_{1g} and E_g channels. A_{2g} and B_{2g} states are not competitive anywhere in the phase diagram. A B_{1g} state is sometimes found as a subleading instability. The E_g solution is dominated by the $\{[6,3],-[5,3]\}$ channel and is stabilized for $t_{56z}^{\mathrm{SOC}} \gtrsim \eta/4$. Under the constraint of realistic Fermi surfaces, the E_g state can be stabilized for t_{56z}^{SOC} as small as about 5 meV, although this requires a rather small value of the on-site SOC. It is remarkable that such a small energy scale determines the relative stability of qualitatively different pairing states. As shown in Fig. 1(b), the Fermi surfaces for parameters stabilizing A_{1g} or E_g states are indeed very similar. The SOC strength remains controversial [48,57,62], but here we have shown its importance for the determination of the most stable superconducting state. Our results are a proof of principle that an E_g superconducting state can be realized in Sr_2RuO_4, even for purely local interactions, once one properly takes into account a complete and plausible 3D model for the normal state.

Figure 2 displays the projected gaps at the Fermi surfaces for representative A_{1g} and E_g states. Note that in both cases the gap magnitude on the α sheet is very small, whereas the gaps

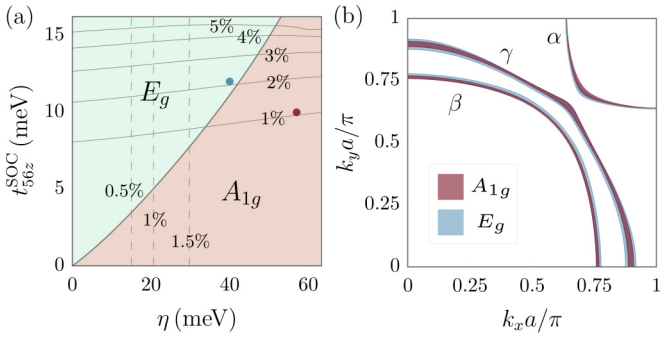

FIG. 1. (a) Phase diagram showing the stability of A_{1g} and E_g pairing states as a function of the SOC parameters η and t_{56z}^{SOC}. The vertical dashed lines indicate the minimum distance between two Fermi surfaces. Percentages are defined as fractions of $2\pi/a$. For small η, the separation between the β and γ bands becomes too small, in view of the ARPES data [48]. The thin solid lines indicate the maximum variation of the Fermi surface along the k_z direction. For large t_{56z}^{SOC}, the Fermi surfaces become too dispersive. The blue and magenta dots denote the parameter choices for E_g and A_{1g} stable solutions used in (b). (b) Fermi-surface shapes, projected onto the $k_x k_y$ plane, for representative points in the A_{1g} (red) and E_g (blue) regions in (a). For A_{1g}, $\eta = 57$ meV and $t_{56z}^{\mathrm{SOC}} = 10$ meV, while for E_g, $\eta = 40$ meV and $t_{56z}^{\mathrm{SOC}} = 12$ meV.

on the β and γ sheets are comparable. This shows that we cannot simply identify the γ band [64] or the pair of almost one-dimensional α and β bands [16] as the dominant ones for superconductivity [19].

It is possible to understand why these SOC terms stabilize the respective ground states based on the notion of superconducting fitness [52,53]. In particular, it has been shown for two-band superconductors that if the quantity $\hat{F}_A(\boldsymbol{k}) = \tilde{H}_0(\boldsymbol{k})\hat{\Delta}(\boldsymbol{k}) + \hat{\Delta}(\boldsymbol{k})\tilde{H}_0^*(-\boldsymbol{k})$ is zero, there is no intraband

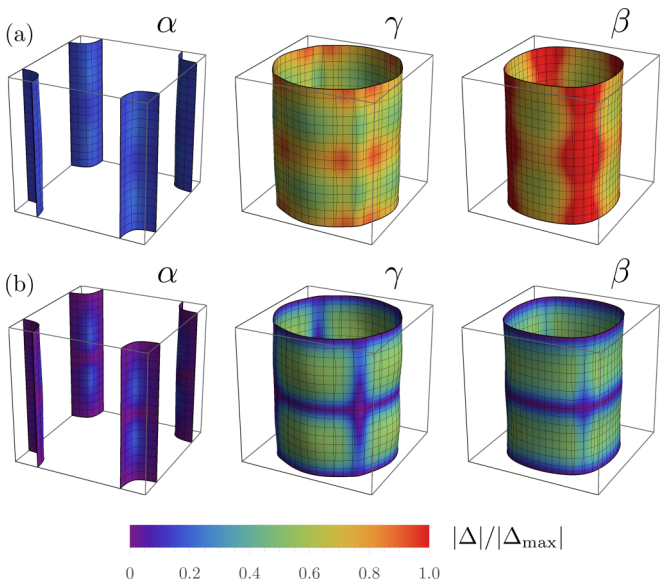

FIG. 2. Projected gaps at the Fermi surfaces for a representative (a) A_{1g} and (b) chiral E_g state in the first Brillouin zone. Parameters are the same as in Fig. 1(b). The color code is normalized to the maximum value of the A_{1g} gap.

pairing and hence no weak-coupling instability [here, $\tilde{H}_0(\boldsymbol{k})$ corresponds to $\hat{H}_0(\boldsymbol{k})$ with $h_{00}(\boldsymbol{k})$ set to zero]. Hence, adding terms to the normal-state Hamiltonian such that $\hat{F}_A(\boldsymbol{k})$ becomes nonzero for a particular gap function turns on a weak-coupling instability in this channel. The fitness analysis can be extended to our three-orbital model or, alternatively, we can construct an effective two-orbital model valid sufficiently far from the Brillouin-zone diagonals. Applying the fitness argument to the effective two-band model, we find that the on-site SOC η turns on both the A_{1g} and B_{1g} pairing channels, whereas the parameter t_{56z}^{SOC} turns on the E_g $\{[6,3],-[5,3]\}$ channel, consistent with what we find numerically. Details of the fitness analysis are given in the SM [58].

In view of the Knight-shift experiments [31,32], it is important to comment on the spin susceptibility associated with the dominant E_g $\{[6,3],-[5,3]\}$ channel. Since it is a spin-triplet state with in-plane spin polarization of the Copper pairs, similar to the familiar chiral p-wave spin-triplet pairing with a $\boldsymbol{d}$ vector along the k_z direction, it might naively be expected to show a temperature-independent spin susceptibility for in-plane fields. This is not the case, however, since the even parity of E_g implies that the intraband pairing potential is a pseudospin singlet when expressed in the band basis and the low-energy response to a magnetic field is identical to a true spin singlet. This has been examined numerically for similar pairing states [45,65], where it was found that only a small fraction of the normal-state spin susceptibility persists at zero temperature in the superconducting state.

Bogoliubov Fermi surfaces. An E_g state is expected to have horizontal line nodes at $k_z = 0$ and $2\pi/c$ [21,36], and it will have vertical line nodes in a time-reversal invariant nematic state [34,36]. Although recent tunneling measurements have called into question time-reversal symmetry breaking in Sr_2RuO_4 [66], here we follow the indications of polar Kerr and μSR experiments [3,4,33], and explicitly consider a chiral E_g state which has no vertical line nodes. It has recently been shown that for an even-parity superconductor that spontaneously breaks time-reversal symmetry, the excitation spectrum is either fully gapped or contains Bogoliubov Fermi surfaces (BFSs) [54,55]. Indeed, the chiral E_g state considered here has BFSs, which are shown in Fig. 3. These BFSs are very thin in the direction perpendicular to the normal-state Fermi surface, giving them a ribbonlike appearance that extends along the k_z axis by about 0.2% of the Brillouin zone. This value is proportional to the gap amplitude, here set to 0.15 meV. While the total residual density of states from the BFSs is not large and may be difficult to observe [67], such a nodal structure implies that some experimental results require reinterpretation. In particular, given that the BFSs extend along the k_z axis, the argument that thermal conductivity measurements rule out the E_g state because it has horizontal line nodes [24] no longer applies. The presence of BFSs may also require a reinterpretation of quasiparticle-interference experiments [68]. We leave a detailed study of experimental consequences of the E_g OAST state for future work.

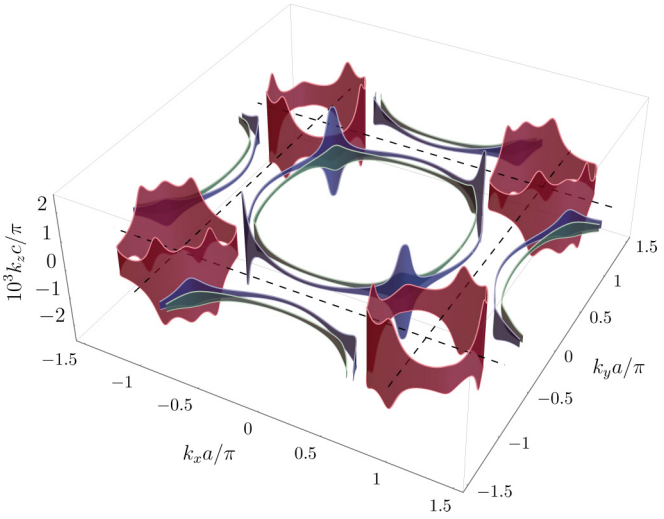

FIG. 3. BFSs for the chiral E_g state. The Fermi surfaces in red, green, and blue correspond to inflated nodes stemming from the α, β, and γ band, respectively.

Conclusions. We have argued that an E_g order parameter can be a realistic weak-coupling ground state for Sr_2RuO_4, once we consider a complete 3D model for the normal state and interactions of the Hubbard-Kanamori type. Key to our construction are the usually neglected momentum-dependent SOC terms in the normal state. These terms can completely change the nature of the superconducting ground state, despite being so small that they do not significantly change the Fermi surfaces. Our theory reconciles the recent observation of a singletlike spin susceptibility with measurements indicating a two-component order parameter and broken time-reversal symmetry.

Acknowledgments. The authors thank A. V. Chubukov and B. Ramshaw for useful discussions. H.M. and P.M.R.B. were supported by the Marsden Fund Council from Government funding, managed by Royal Society Te Apārangi. A.R. acknowledges the support of Fundação de Amparo à Pesquisa do Estado de São Paulo (FAPESP) Project No. 2018/18287-8, and Fundação para o Desenvolvimento da UNESP (FUNDUNESP) Process No. 2338/2014-CCP. C.T. acknowledges financial support by the Deutsche Forschungsgemeinschaft through the Collaborative Research Center SFB 1143, Project A04, the Research Training Group GRK 1621, and the Cluster of Excellence on Complexity and Topology in Quantum Matter ct.qmat (EXC 2147).

H.G.S. and H.M. contributed equally to this work.

[1] K. Ishida, H. Mukuda, Y. Kitaoka, K. Asayama, Z. Q. Mao, Y. Mori, and Y. Maeno, Spin-triplet superconductivity in Sr_2RuO_4 identified by ^{17}O Knight shift, Nature (London) **396**, 658 (1998).

[2] J. A. Duffy, S. M. Hayden, Y. Maeno, Z. Mao, J. Kulda, and G. J. McIntyre, Polarized-Neutron Scattering Study of the Cooper-Pair Moment in Sr_2RuO_4, Phys. Rev. Lett. **85**, 5412 (2000).

[3] G. M. Luke, Y. Fudamoto, K. M. Kojima, M. I. Larkin, J. Merrin, B. Nachumi, Y. J. Uemura, Y. Maeno, Z. Q. Mao, Y. Mori, H. Nakamura, and M. Sigrist, Time-reversal symmetry breaking superconductivity in Sr_2RuO_4, Nature (London) **394**, 558 (1998).

[4] J. Xia, Y. Maeno, P. T. Beyersdorf, M. M. Fejer, and A. Kapitulnik, High Resolution Polar Kerr Effect Measurements in Sr_2RuO_4: Evidence for Broken Time-Reversal Symmetry in the Superconducting State, Phys. Rev. Lett. **97**, 167002 (2006).

[5] Y. Maeno, H. Hashimoto, K. Yoshida, S. Nishizaki, T. Fujita, J. G. Bednorz, and F. Lichtenberg, Superconductivity in a layered perovskite without copper, Nature (London) **372**, 532 (1994).

[6] T. M. Rice and M. Sigrist, Sr_2RuO_4: An electronic analogue of ^{3}He? J. Phys.: Condens. Matter **7**, L643 (1995).

[7] I. I. Mazin and D. J. Singh, Competitions in Layered Ruthenates: Ferromagnetism Versus Antiferromagnetism and Triplet Versus Singlet Pairing, Phys. Rev. Lett. **82**, 4324 (1999).

[8] K. Miyake and O. Narikiyo, Model for Unconventional Superconductivity of Sr_2RuO_4: Effect of Impurity Scattering on Time-Reversal Breaking Triplet Pairing with a Tiny Gap, Phys. Rev. Lett. **83**, 1423 (1999).

[9] T. Kuwabara and M. Ogata, Spin-Triplet Superconductivity Due to Antiferromagnetic Spin-Fluctuation in Sr_2RuO_4, Phys. Rev. Lett. **85**, 4586 (2000).

[10] M. Sato and M. Kohmoto, Mechanism of spin-triplet superconductivity in Sr_2RuO_4, J. Phys. Soc. Jpn. **69**, 3505 (2000).

[11] T. Takimoto, Orbital fluctuation-induced triplet superconductivity: Mechanism of superconductivity in Sr_2RuO_4, Phys. Rev. B **62**, R14641(R) (2000).

[12] T. Nomura and K. Yamada, Roles of electron correlations in the spin-triplet superconductivity of Sr_2RuO_4, J. Phys. Soc. Jpn. **71**, 1993 (2002).

[13] Y. Yanase and M. Ogata, Microscopic identification of the d-vector in triplet superconductor Sr_2RuO_4, J. Phys. Soc. Jpn. **72**, 673 (2003).

[14] J. F. Annett, G. Litak, B. L. Gyorffy, and K. I. Wysokinski, Spin-orbit coupling and symmetry of the order parameter in strontium ruthenate, Phys. Rev. B **73**, 134501 (2006).

[15] Y. Yoshioka and K. Miyake, Pairing mechanism and anisotropy of d-vector of spin-triplet superconductor Sr_2RuO_4, J. Phys. Soc. Jpn. **78**, 074701 (2009).

[16] S. Raghu, A. Kapitulnik, and S. A. Kivelson, Hidden Quasi-One-Dimensional Superconductivity in Sr_2RuO_4, Phys. Rev. Lett. **105**, 136401 (2010).

[17] Q. H. Wang, C. Platt, Y. Yang, C. Honerkamp, F. C. Zhang, W. Hanke, T. M. Rice, and R. Thomale, Theory of superconductivity in a three-orbital model of Sr_2RuO_4, Europhys. Lett. **104**, 17013 (2013).

[18] J.-W. Huo, T. M. Rice, and F. C. Zhang, Spin Density Wave Fluctuations and p-Wave Pairing in Sr_2RuO_4, Phys. Rev. Lett. **110**, 167003 (2013).

[19] T. Scaffidi, J. C. Romers, and S. H. Simon, Pairing symmetry and dominant band in Sr_2RuO_4, Phys. Rev. B **89**, 220510(R) (2014).

[20] M. Tsuchiizu, Y. Yamakawa, S. Onari, Y. Ohno, and H. Kontani, Spin-triplet superconductivity in Sr_2RuO_4 due to orbital and spin fluctuations: Analyses by two-dimensional renormalization group theory and self-consistent vertex-correction method, Phys. Rev. B **91**, 155103 (2015).

[21] A. P. Mackenzie, T. Scaffidi, C. W. Hicks, and Y. Maeno, Even odder after twenty-three years: The superconducting order parameter puzzle of Sr_2RuO_4, njp Quantum Mater. **2**, 40 (2017).

[22] J. R. Kirtley, C. Kallin, C. W. Hicks, E.-A. Kim, Y. Liu, K. A. Moler, Y. Maeno, and K. D. Nelson, Upper limit on spontaneous supercurrents in Sr_2RuO_4, Phys. Rev. B **76**, 014526 (2007).

[23] C. Lupien, W. A. MacFarlane, C. Proust, L. Taillefer, Z. Q. Mao, and Y. Maeno, Ultrasound Attenuation in Sr_2RuO_4: An Angle-Resolved Study of the Superconducting Gap Function, Phys. Rev. Lett. **86**, 5986 (2001).

[24] E. Hassinger, P. Bourgeois-Hope, H. Taniguchi, S. René de Cotret, G. Grissonnanche, M. S. Anwar, N. Doiron-Leyraud, and L. Taillefer, Vertical Line Nodes in the Superconducting Gap Structure of Sr_2RuO_4, Phys. Rev. X **7**, 011032 (2017).

[25] S. Kittaki, S. Nakamura, T. Sakakibara, N. Kikugawa, T. Terashima, S. Uji, D. Sokolov, A. P. Mackenzie, K. Irie, Y. Tsutsumi, K. Suzuki, and K. Machida, Searching for gap zeros in Sr_2RuO_4 via field-angle-dependent specific-heat measurement, J. Phys. Soc. Jpn. **87**, 093703 (2018).

[26] S. Kittaka, A. Kasahara, T. Sakakibara, D. Shibata, S. Yonezawa, Y. Maeno, K. Tenya, and K. Machida, Sharp magnetization jump at the first-order superconducting transition in Sr_2RuO_4, Phys. Rev. B **90**, 220502 (2014).

[27] C. W. Hicks, D. O. Brodsky, E. A. Yeland, A. S. Gibbs, J. A. N. Bruin, M. E. Barber, S. D. Edkins, K. Nishimura, S. Yonezawa, Y. Maeno, and A. P. Mackenzie, Strong increase in T_c of Sr_2RuO_4 under both tensile and compressive strain, Science **344**, 283 (2014).

[28] A. Steppke, L. Zhao, M. E. Barber, T. Scaffidi, F. Jerzembeck, H. Rosner, A. S. Gibbs, Y. Maeno, S. H. Simon, A. P. Mackenzie, and C. W. Hicks, Strong peak in T_c of Sr_2RuO_4 under uniaxial pressure, Science **355**, eaaf9398 (2017).

[29] C. Kallin and A. J. Berlinsky, Is Sr_2RuO_4 a chiral p-wave superconductor? J. Phys.: Condens. Matter **21**, 164210 (2009).

[30] S. B. Etter, A. Bouhon, and M. Sigrist, Spontaneous surface flux pattern in chiral p-wave superconductors, Phys. Rev. B **97**, 064510 (2018).

[31] A. Pustogow, Y. Luo, A. Chronister, Y. S. Su, D. A. Sokolov, F. Jerzembeck, A. P. Mackenzie, C. W. Hicks, N. Kikugawa, S. Raghu, E. D. Bauer, and S. E. Brown, Constraints on the superconducting order parameter in Sr_2RuO_4 from oxygen-17 nuclear magnetic resonance, Nature (London) **574**, 72 (2019).

[32] K. Ishida, M. Manago, and Y. Maeno, Reduction of the ^{17}O Knight shift in the superconducting state and the heat-up effect by NMR pulses on Sr_2RuO_4, J. Phys. Soc. Jpn. **89**, 034712 (2020).

[33] V. Grinenko, S. Ghosh, R. Sarkar, J.-C. Orain, A. Nikitin, M. Elender, D. Das, Z. Guguchia, F. Brückner, M. E. Barber, J. Park, N. Kikugawa, D. A. Sokolov, J. S. Bobowski, T. Miyoshi, Y. Maeno, A. P. Mackenzie, H. Luetkens, C. W. Hicks, and H.-H. Klauss, Split superconducting and time-reversal symmetry-breaking transitions, and magnetic order in Sr_2RuO_4 under uniaxial stress, arXiv:2001.08152.

[34] S. Benhabib, C. Lupien, I. Paul, L. Berges, M. Dion, M. Nardone, A. Zitouni, Z. Q. Mao, Y. Maeno, A. Georges, L. Taillefer, and C. Proust, Jump in the c_{66} shear modulus at the superconducting transition of Sr_2RuO_4: Evidence for a two-component order parameter, arXiv:2002.05916.

[35] S. Ghosh, A. Shekhter, F. Jerzembeck, N. Kikugawa, D. A. Sokolov, M. Brando, A. P. Mackenzie, C. W. Hicks, and

B. J. Ramshaw, Thermodynamic evidence for a two-component superconducting order parameter in Sr_2RuO_4, arXiv:2002.06130.

[36] M. Sigrist and K. Ueda, Phenomenological theory of unconventional superconductivity, Rev. Mod. Phys. **63**, 239 (1991).

[37] I. Žutić and I. I. Mazin, Phase-Sensitive Tests of the Pairing State Symmetry in Sr_2RuO_4, Phys. Rev. Lett. **95**, 217004 (2005).

[38] H. S. Røising, T. Scaffidi, F. Flicker, G. F. Lange, and S. H. Simon, Superconducting order of Sr_2RuO_4 from a three-dimensional microscopic model, Phys. Rev. Research **1**, 033108 (2019).

[39] I. Schnell, I. I. Mazin, and A. Y. Liu, Unconventional superconducting pairing symmetry induced by phonons, Phys. Rev. B **74**, 184503 (2006).

[40] C. M. Puetter and H.-Y. Kee, Identifying spin-triplet pairing in spin-orbit coupled multi-band superconductors, Europhys. Lett. **98**, 27010 (2012).

[41] J. Spałek, Spin-triplet superconducting pairing due to local Hund's rule and Dirac exchange, Phys. Rev. B **63**, 104513 (2001).

[42] J. E. Han, Spin-triplet *s*-wave local pairing induced by Hund's rule coupling, Phys. Rev. B **70**, 054513 (2004).

[43] O. Vafek and A. V. Chubukov, Hund Interaction, Spin-Orbit Coupling, and the Mechanism of Superconductivity in Strongly Hole-Doped Iron Pnictides, Phys. Rev. Lett. **118**, 087003 (2017).

[44] A. K. C. Cheung and D. F. Agterberg, Superconductivity in the presence of spin-orbit interactions stabilized by Hund coupling, Phys. Rev. B **99**, 024516 (2019).

[45] A. W. Lindquist and H.-Y. Kee, Distinct reduction of Knight shift in superconducting state of Sr_2RuO_4 under uniaxial strain, arXiv:1912.02215.

[46] S. Hoshino and P. Werner, Superconductivity from Emerging Magnetic Moments, Phys. Rev. Lett. **115**, 247001 (2015).

[47] O. Gingras, R. Nourafkan, A.-M. S. Tremblay, and M. Côté, Superconducting Symmetries of Sr_2RuO_4 from First-Principles Electronic Structure, Phys. Rev. Lett. **123**, 217005 (2019).

[48] A. Tamai, M. Zingl, E. Rozbicki, E. Cappelli, S. Riccò, A. de la Torre, S. McKeown Walker, F. Y. Bruno, P. D. C. King, W. Meevasana, M. Shi, M. Radović, N. C. Plumb, A. S. Gibbs, A. P. Mackenize, C. Berthod, H. U. R. Strand, M. Kim, A. Georges, and F. Baumberger, High-Resolution Photoemission on Sr_2RuO_4 Reveals Correlation-Enhanced Effective Spin-Orbit Coupling and Dominantly Local Self-Energies, Phys. Rev. X **9**, 021048 (2019).

[49] L. Fu and E. Berg, Odd-Parity Topological Superconductors: Theory and Application to $Cu_xBi_2Se_2$, Phys. Rev. Lett. **105**, 097001 (2010).

[50] S. Sasaki, M. Kriener, K. Segawa, K. Yada, Y. Tanaka, M. Sato, and Y. Ando, Topological Superconductivity in $Cu_xBi_2Se_3$, Phys. Rev. Lett. **107**, 217001 (2011).

[51] A. Yamakage, K. Yada, M. Sato, and Y. Tanaka, Theory of tunneling conductance and surface-state transition in superconducting topological insulators, Phys. Rev. B **85**, 180509(R) (2012).

[52] A. Ramires and M. Sigrist, Identifying detrimental effects for multi-orbital superconductivity: Application to Sr_2RuO_4, Phys. Rev. B **94**, 104501 (2016).

[53] A. Ramires, D. F. Agterberg, and M. Sigrist, Tailoring T_c by symmetry principles: The concept of superconducting fitness, Phys. Rev. B **98**, 024501 (2018).

[54] D. F. Agterberg, P. M. R. Brydon, and C. Timm, Bogoliubov Fermi Surfaces in Superconductors with Broken Time-Reversal Symmetry, Phys. Rev. Lett. **118**, 127001 (2017).

[55] P. M. R. Brydon, D. F. Agterberg, H. Menke, and C. Timm, Bogoliubov Fermi surfaces: General theory, magnetic order, and topology, Phys. Rev. B **98**, 224509 (2018).

[56] A. Ramires and M. Sigrist, Superconducting order parameter of Sr_2RuO_4: A microscopic perspective, Phys. Rev. B **100**, 104501 (2019).

[57] C. N. Veenstra, Z.-H. Zhu, M. Raichle, B. M. Ludbrook, A. Nicolaou, B. Slomski, G. Landolt, S. Kittaka, Y. Maeno, J. H. Dil, I. S. Elfimov, M. W. Haverkort, and A. Damascelli, Spin-Orbital Entanglement and the Breakdown of Singlets and Triplets in Sr_2RuO_4 Revealed by Spin- and Angle-Resolved Photoemission Spectroscopy, Phys. Rev. Lett. **112**, 127002 (2014).

[58] See Supplemental Material at http://link.aps.org/supplemental/10.1103/PhysRevResearch.2.032023 for details on the construction of the tight-binding model, the linearized gap equation, and the fitness analysis, which includes Refs. [59–61].

[59] M. Gradhand, K. I. Wysokinski, J. F. Annett, and B. L. Györffy, Kerr rotation in the unconventional superconductor Sr_2RuO_4, Phys. Rev. B **88**, 094504 (2013).

[60] W. Huang and H. Yao, Possible Three-Dimensional Nematic Odd-Parity Superconductivity in Sr_2RuO_4, Phys. Rev. Lett. **121**, 157002 (2018).

[61] D. E. King, Dlib-ml: A machine learning toolkit, J. Mach. Learn. Res. **10**, 1755 (2009).

[62] G. Zhang, E. Gorelov, E. Sarvestani, and E. Pavarini, Fermi Surface of Sr_2RuO_4: Spin-Orbit and Anisotropic Coulomb Interaction Effects, Phys. Rev. Lett. **116**, 106402 (2016).

[63] E. Dagotto, T. Hotta, and A. Moreo, Colossal magnetoresistant materials: The key role of phase separation, Phys. Rep. **344**, 1 (2001).

[64] D. F. Agterberg, M. Sigrist, and T. M. Rice, Orbitally Dependent Superconductivity in Sr_2RuO_4, Phys. Rev. Lett. **78**, 3374 (1997).

[65] Y. Yu, A. K. C. Cheung, S. Raghu, and D. F. Agterberg, Residual spin susceptibility in the spin-triplet orbital-singlet model, Phys. Rev. B **98**, 184507 (2018).

[66] S. Kashiwaya, K. Saitoh, H. Kashiwaya, M. Koyanagi, M. Sato, K. Yada, Y. Tanaka, and Y. Maeno, Time-reversal invariant superconductivity of Sr_2RuO_4 revealed by Josephson effects, Phys. Rev. B **100**, 094530 (2019).

[67] C. J. Lapp, G. Börner, and C. Timm, Experimental consequences of Bogoliubov Fermi surfaces, Phys. Rev. B **101**, 024505 (2020).

[68] R. Sharma, S. D. Edkins, Z. Wang, A. Kostin, C. Sow, Y. Maeno, A. P. Mackenzie, J. C. S. Davis, and V. Madhavan, Momentum resolved superconducting energy gaps of Sr_2RuO_4 from quasiparticle interference imaging, Proc. Natl. Acad. Sci. USA **117**, 5222 (2020).